



HAL
open science

**Solid-state and solution characterizations of
[(TMPA)Cu(II)(SO₃)] and [(TMPA)Cu(II)(S₂O₃)]
complexes: Application to sulfite and thiosulfate fast
detection**

Léonie Berthonnaud, Charlène Esmieu, Sonia Mallet-Ladeira, Christelle
Hureau

► **To cite this version:**

Léonie Berthonnaud, Charlène Esmieu, Sonia Mallet-Ladeira, Christelle Hureau. Solid-state and solution characterizations of [(TMPA)Cu(II)(SO₃)] and [(TMPA)Cu(II)(S₂O₃)] complexes: Application to sulfite and thiosulfate fast detection. *Journal of Inorganic Biochemistry*, 2021, 225, pp.111601. 10.1016/j.jinorgbio.2021.111601 . hal-03394471

HAL Id: hal-03394471

<https://hal.science/hal-03394471v1>

Submitted on 22 Oct 2021

HAL is a multi-disciplinary open access archive for the deposit and dissemination of scientific research documents, whether they are published or not. The documents may come from teaching and research institutions in France or abroad, or from public or private research centers.

L'archive ouverte pluridisciplinaire **HAL**, est destinée au dépôt et à la diffusion de documents scientifiques de niveau recherche, publiés ou non, émanant des établissements d'enseignement et de recherche français ou étrangers, des laboratoires publics ou privés.

Solid-state and solution characterizations of [(TMPA)Cu(II)(SO₃)] and [(TMPA)Cu(II)(S₂O₃)] complexes: application to sulfite and thiosulfate fast detection.

Léonie Berthonnaud;^{a,b} Charlène Esmieu;^a Sonia Mallet-Ladeira;^a Christelle Hureau^{a,*}

a. LCC-CNRS, Université de Toulouse, CNRS, Toulouse, France christelle.hureau@lcc-toulouse.fr

b. Division of Materials Science, Nara Institute of Science and Technology. 8916-5 Takayama, Ikoma, Nara, Japan

Abstract

Sulfite (SO₃²⁻) and thiosulfate (S₂O₃²⁻) ions are used as food preservative and antichlor agent respectively. To detect low levels of such anions we used Cu(II) complex of the Tris-Methyl Pyridine Amine (TMPA) ligand, denoted L. Formation of [LCu(SO₃)] (**1**) and [LCu(S₂O₃)] (**2**) in solution were monitored using UV-Vis, EPR and cyclic voltammetry, while the solid-state X-ray structures of both complexes were solved. In addition, we also evaluated the pH range in which the complexes are stable, and the anions binding affinity values for the [LCu(solvent)]²⁺ (**3**) parent complex. As a matter of illustration, we determined the sulfite content in a commercial crystal sugar.

Keywords :

- Copper(II)
- TMPA
- Sulfite
- Thiosulfate
- EPR
- UV-vis

Introduction

Copper is an essential element in biology,¹ being present in many key enzymes, such as in Cytochrome C oxidase (CcO) that provides the four-electron-four-proton-reduction of dioxygen to water leading to the formation of a proton gradient across the cellular membrane and ultimately to the biosynthesis of ATP.² In CcO, the hetero-binuclear catalytic center is provided by a heme and a copper-bound to three N-ligands from side-chains of Histidine (His) residues, while the dioxygen substrate bridges the two metallic centers.³ Many bioinspired models of CcO have been developed in the last 30 years.^{3, 4} In several of them, the copper first coordination sphere was mimicked using 4N-containing tripodal ligands. Among them the multi-functions ligand TMPA (Tris-Methyl Pyridine Amine, also reported as TPA and TPMA)⁵ is the one of the most, if not the most studied ligand. In addition to its potential in CcO modelling, Cu(TMPA) and its derivatives have been used for the investigations of dioxygen activation using mononuclear model (for recent examples, see for instance refs. ⁶⁻¹¹). This was the motivation for the use of this ligand in our research that aims at evaluating dioxygen activation by Cu-peptide complexes.^{12, 13} In this context Cu(TMPA) complex would have served as a widely-recognized reference for dioxygen activation. In the course of our experiments, we evidenced that the Cu(TMPA) complex can also be a very interesting probe for the detection of sulfite and thiosulfate ions and this is what we will mainly describe in the present report.

Sulfite (E221) ion is well-known food and beverages additive, used as preservative agent to counteract food evolution and browning.^{14, 15} Thiosulfate (E539, also known as hyposulfite) ion is used to neutralize the effects of chlorine used for water treatment, bleaching in paper and textile industries and as highly specific medications.¹⁶ A tuned balance is required since excess of sulfite has unwanted side-effects for health such as allergic reaction and asthma;¹⁷ the daily consumption is thus limited (below 0.7 mg/kg of body weight).¹⁸ Hence, the need for probes to detect sulfite ions and to a lesser extent thiosulfate ions. Although they are already available techniques to detect sulfite and thiosulfate ions,¹⁹ it is interesting to complete them with easy-to-use probes and detection methods.

The full characterization of [LCu(SO₃)] (**1**) and [LCu(S₂O₃)] (**2**) in solid state by X-ray crystallography and in solution by various methods (UV-Vis, EPR and cyclic voltammetry) together with the speciation of the two complexes as a function of pH, and the evaluation of the affinity of SO₃²⁻ and S₂O₃²⁻ for [LCu(solvent)]²⁺ (**3**) are described in the present report. Then, the use of **3** to detect sulfite ions in crystal sugar is reported and briefly discussed with respect to other current methods, while a short description on how we serendipitously detected species **1** is also given.

X-ray crystallographic studies of [LCu(SO₃)] (**1**), [LCu(S₂O₃)] (**2**)

An ORTEP representation of the structures of [LCu(SO₃)] (**1**) and [LCu(S₂O₃)] (**2**) is given in Figure 1 and crystallographic details of the structures are given in Table S1. Selected bond distances and angles are listed in Tables 1, S2 and S3, where they are compared with those of [LCu(H₂O)]²⁺,²⁰⁻²⁴ [LCu(AcN)]²⁺ (AcN = acetonitrile)²⁵⁻²⁷ (Table 1), and [L_TCu(S₂O₃)]²⁸ where L_T is a ligand from the tren (tris(2-methylaminoethyl)amine) family, namely tren, Me₃tren and Bz₃tren (Tables S2 and S3). The empirical Addison parameter τ is a very useful tool to compare geometries of penta-coordinated structures. It is defined by $\tau = (\text{difference between the 2 largest L-M-L angles})/60$. When $\tau = 1$ the complex geometry is trigonal bipyramidal (TBP) and when $\tau = 0$ it is square pyramidal (SQ).²⁹

1 has a nearly perfect TBP geometry ($\tau = 1$) as have the two parent complexes [LCu(H₂O)]²⁺, [LCu(AcN)]²⁺ with $\tau = 0.94$ and $\tau = 0.84$, respectively (Table 1). The equatorial angles are similar and close to 120°. The angle S(1)-Cu-N(2) is close to linearity with 178.9°. All the Cu-N bond distances are comparable (2.07 Å - 2.09 Å) except the Cu-S(1) bond distance that is longer (2.25 Å) in line with binding to bulky sulfur atom, while the O and N atoms of [LCu(H₂O)]²⁺ and [LCu(AcN)]²⁺ respectively are much closer (1.95 Å and 1.98 Å). The angles N(2)-Cu-N_{eq} are less than 90°, the Cu(II) center is thus out of the equatorial plane toward the sulfite ion. Similar trends were also observed for [LCu(H₂O)]²⁺ and [LCu(AcN)]²⁺ (Table 1) and thus is not linked to the nature of the exogenous ligand. To the best of our knowledge, there is no X-ray structure of a Cu(II)-sulfite complex.

2 has an intermediate structure because of the O(1) atom from the thiosulfate ion that is not bound to the Cu(II) center (Cu-O(1) distance equals 2.70 Å), but occupies the sixth position of an octahedron. Hence, this interaction induces a high distortion in the classical TBP toward square pyramidal (SP) geometry with $\tau = 0.11$, also characterized by an elongation of the Cu-N(3) bond distance (2.20 Å) in trans to the O(1) atom. Such SP geometry has only been reported once for one of the two inequivalent complexes characterized in the X-ray structures of [(Me₃tren)Cu(S₂O₃)]. Otherwise, the geometry around [(tren)Cu(S₂O₃)]²⁺, [(Bz₃tren)Cu(S₂O₃)]²⁺ and [(Me₃tren)Cu(RS₂O₂)]²⁺ (R=Me, Ph and MePh)³⁰ are TBP. Such an unusual coordination might be due to crystal packing. The N(3)-Cu(II) bond thus represents the axial direction, with the equatorial plane defined by the other three N and S(1) atoms. Indeed, the angles S(1)-Cu-N(2) and N(1)-Cu-N(4) are approaching linearity with 168.1 Å and 161.6 Å, respectively. The Cu-S(1) bond distance of 2.29 Å is in the same range as the one in **1** and the [L_TCu(S₂O₃)] parent complexes.

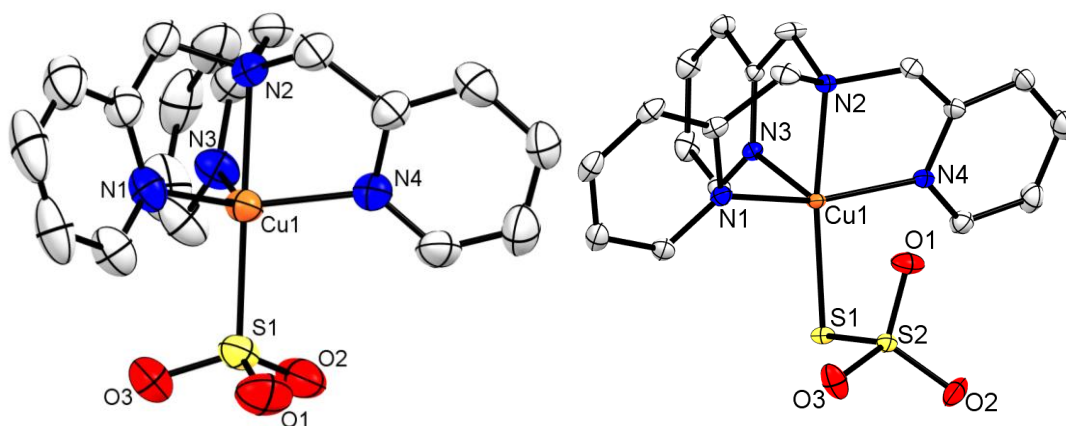


Figure 1. X-ray structures of $\text{LCu}(\text{SO}_3)$ (**1**), $\text{LCu}(\text{S}_2\text{O}_3)$ (**2**) drawn with 50% of ellipsoid.

Table 1. Selected distances (Å) and angles (°) for **1** and **2**. The longest distances are shown in bold.

| | 1 | 2 | $[\text{LCu}(\text{H}_2\text{O})]^{2+}$ ^[a] | $[\text{LCu}(\text{CH}_3\text{CN})]^{2+}$ ^[a] |
|--|-----------------|------------------|--|--|
| Cu-N(1) | 2.071(7) | 2.029(1) | 2.071(1) | 2.042(5) |
| Cu-N(2) | 2.087(7) | 2.0618(9) | 2.006(1) | 2.021(4) |
| Cu-N(3) | 2.078(7) | 2.2025(9) | 2.059(1) | 2.082(4) |
| Cu-N(4) | 2.086(7) | 2.0417(9) | 2.061(1) | 2.025(5) |
| Cu-S(1)/O _w /N _{AcN} | 2.253(2) | 2.2878(4) | 1.952(1) | 1.976(5) |
| Cu-O(1) | - | 2.695(1) | - | - |
| S(1)/O _w /N _{AcN} -Cu-N(2) | 178.9(2) | 168.09(3) | 176.54(5) | 177.7(2) |
| N(1)-Cu-N(3) | 118.5(3) | 93.95(4) | 117.66(5) | 113.9(2) |
| N(1)-Cu-N(4) | 116.1(3) | 161.62(4) | 117.04(5) | 127.2(2) |
| N(3)-Cu-N(4) | 117.2(3) | 92.80(4) | 119.9(5) | 114.1(2) |
| O(1)-Cu-N3 | - | 173.72(3) | - | - |

^[a] To ease comparison, the N atoms in $[\text{LCu}(\text{H}_2\text{O})]^{2+}$ and $[\text{LCu}(\text{AcN})]^{2+}$ have been labelled according to the present convention (N(2) for amine nitrogen atom and N(1), N(3) and N(4) for pyridine nitrogen atoms).

Solution characterizations of SO_3^{2-} and $\text{S}_2\text{O}_3^{2-}$ interactions with $[\text{LCu}(\text{solvent})]^{2+}$

UV-Vis and EPR characterizations

The UV-Visible and EPR spectra of *in situ* generated complexes **1**, **2** and the reference $[\text{LCu}(\text{solvent})]^{2+}$ (**3**) are reported in Figure 2 panel A and B, respectively. In the d-d region of the UV-Vis spectra and in EPR, the three species have different fingerprints, mirroring a different environment around the Cu(II) center. **1** – **3** have UV-Vis transition bands characteristic of a TBP geometry with an intense peak in the near-infrared region at 750 nm ($\epsilon = 390 \text{ M}^{-1}\text{cm}^{-1}$), 935 nm ($\epsilon = 180 \text{ M}^{-1}\text{cm}^{-1}$) and 870 nm ($\epsilon = 230 \text{ M}^{-1}\text{cm}^{-1}$), respectively, and a higher energy band at 573 nm ($\epsilon = 490 \text{ M}^{-1}\text{cm}^{-1}$) for **1**, 700 nm ($\epsilon = 100 \text{ M}^{-1}\text{cm}^{-1}$) for **2** and an ill-defined shoulder near 680 nm in case of **3** (Table 2). A ligand to Cu(II) charge transfer (LMCT) band is observed for **1** at 430 nm ($\epsilon = 8600 \pm 200 \text{ M}^{-1}\text{cm}^{-1}$) and **2** at 401 nm ($\epsilon = 6000 \pm 200 \text{ M}^{-1}\text{cm}^{-1}$), reminiscent of those observed for the parent complexes $[\text{L}_T\text{Cu}(\text{S}_2\text{O}_3)]$.²⁸

In EPR, the spectra are characteristic of TBP Cu(II) complexes exhibiting a reverse axial pattern ($g_{\perp} > g_{\parallel}$) indicating a d_{z^2} ground state.³¹ This is a quite unusual feature for Cu(II) species that more often lie into elongated octahedral, square planar or square-based pyramid geometries, with $g_{\perp} > g_{\parallel}$.¹ However, it is a fingerprint of Cu(II) complexes of 4N-tripodal ligands.³²⁻³⁶ Although a slight rhombicity can be anticipated (i.e. the situation doesn't exactly correspond to $g_{\perp} = g_x = g_y$), especially in case of **2** and **3**, we will consider the three EPR signatures as axial. Similar patterns have been reported for LCu(II)-based complexes in various solvents and solvent mixtures,^{20, 37-39} and for LCu(II)-oxygen intermediate adducts.^{7, 40-43} The hyperfine couplings can be detected in both perpendicular and parallel directions. We have directly measured them on the spectra (Figure 1B and parameters listed in Table 2). For **1** and **2** the signatures are narrower than in **3**, in line with closer g_{\perp} and g_{\parallel} values. For **1**, the A_{\parallel} is smaller than A_{\perp} while this is the opposite in case of **2** and **3**. For **2** and **3**, the hyperfine lines are broader and less well-defined, mirroring the presence of several species in solution and/or anisotropically strained spectra. Such features are not observed in **1**, in line with a well-defined TBP structure of **1** in solution.

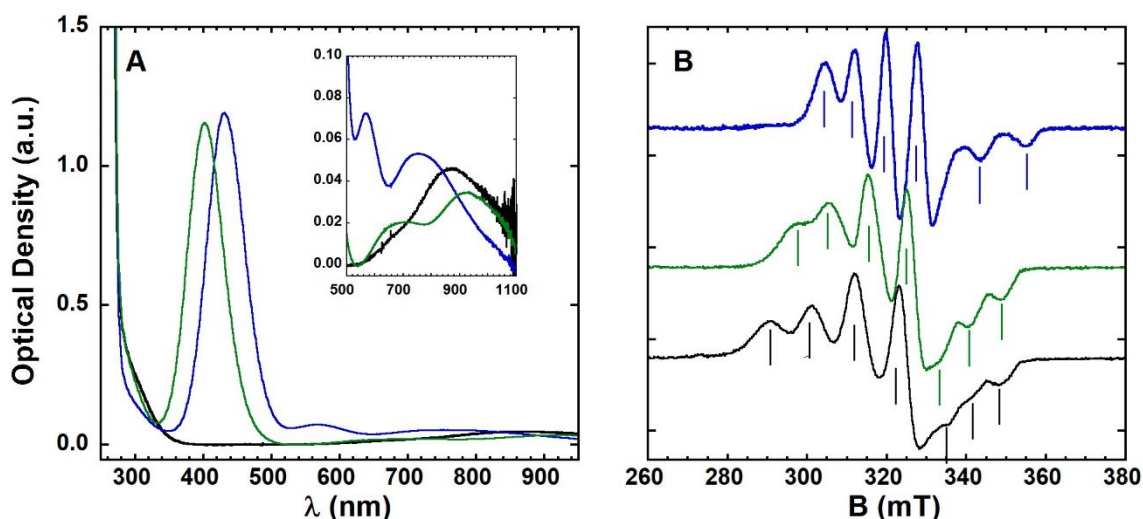


Figure 2. UV-Vis (panel A) and 9-GHz EPR (panel B) of complexes **1** (blue line), **2** (green line) and **3** (black line). Complexes were generated in situ. Panel A: [Cu] = 0.2 mM ; [L] = 0.22 mM ; [SO₃²⁻] = [S₂O₃²⁻] = 1 mM ; AcN/HEPES (pH 6.5) 100 mM (50/50 v/v). $l = 1$ cm; T = 25°C. Panel B: [⁶⁵Cu] = 500 μM; [L] = 550 μM; [SO₃²⁻] = [S₂O₃²⁻] = 2.5 mM in AcN/HEPES (pH 6.5) 100 mM (50/50 v/v). T = 120 K, microwave power: 5 mW.

Table 2. Physico-chemical parameters of complexes **1** – **3** in AcN/HEPES (pH 6.5) 100 mM (50/50 v/v).

| complex | $\lambda_{\max 1}$ (nm) | $\epsilon^{[a]}$ (M ⁻¹ cm ⁻¹) | $\lambda_{\max 2}$ (nm) | $\epsilon^{[a]}$ (M ⁻¹ cm ⁻¹) | pKa ₁ | pKa ₂ | ^{app} Ka (10 ³ M ⁻¹) | $g_{\perp}^{[c]}$ (A _⊥ , 10 ⁴ cm ⁻¹) | $g_{\parallel}^{[c]}$ (A _∥ , 10 ⁴ cm ⁻¹) | E _{1/2} (V. vs SCE) | ΔE ^p (mV) |
|-------------------------|----------------------------|---|----------------------------|---|------------------|------------------|---|--|--|------------------------------------|-------------------------|
| 1 | 430 | 8600 ± 200 | 573 750 | 490 ± 20 390 ± 20 | 6.0 ± 0.1 | 9.5 ± 0.1 | 2.5 ± 0.5 | 2.14 (76) | 2.00 (104) | -0.25 | 100 |
| 2 | 401 | 6000 ± 200 | 700 935 | 100 ± 20 180 ± 20 | 1.6 ± 0.1 | 9.0 ± 0.1 | 40 ± 10 | 2.17 (101) | 2.00 (69) | -0.27 | 90 |
| 3 | | | 680 870 | 80 ± 20 230 ± 20 | | | | 2.21 (110) | 2.00 (60) | -0.21 | 120 |
| 1 ^[b] | 418 | 8200 ± 400 | 665 870 | 80 ± 20 260 ± 20 | | | 7 ± 1 | † | † | † | † |

^[a] The ϵ values of the LMCT and d-d bands were deduced from the fits of the titration curves (See Exp. Section).

^[b] Values in aqueous buffer (HEPES 100 mM, pH 6.5).

^[c] EPR parameters were deduced from the position of the second and third hyperfine lines in the perpendicular plan and along the parallel direction (except for **2**, where the third and four hyperfine parallel lines were used). g values were calculated from the average of the field position of the second and third hyperfine lines, while the hyperfine values correspond to the field differences between these two lines. ⁶⁵Cu isotope was used.

pH stability domains

The pH^[#] domain where complexes **1** and **2** predominate were determined using pH-titration monitored by UV-Vis following the LMCT band. The results are given in Figure 3. From the fits of the curves, the two pKa values corresponding to evolution of the complexes in acidic or basic media were determined (reported in Table 2). The first pKa value of **1** and **2** (6.0 and 1.6) is directly linked to the protonation constants of SO_3^{2-} and $\text{S}_2\text{O}_3^{2-}$ (pKa values of 7.0 and 1.7, respectively). The slightly lower pKa value obtained for **1** versus SO_3^{2-} indicates a stabilization of the SO_3^{2-} protonation state by binding to the Cu(II) ion. The second pKa values of **1** and **2**, which are very close for both dianions, may witness a similar competition between SO_3^{2-} or $\text{S}_2\text{O}_3^{2-}$ and HO^- for Cu(II) binding.

[#] For a matter of simplicity, pH is here used abusively as the experiment is in a mixture of AcN/HEPES (pH 6.5) 100mM (50/50 v/v).

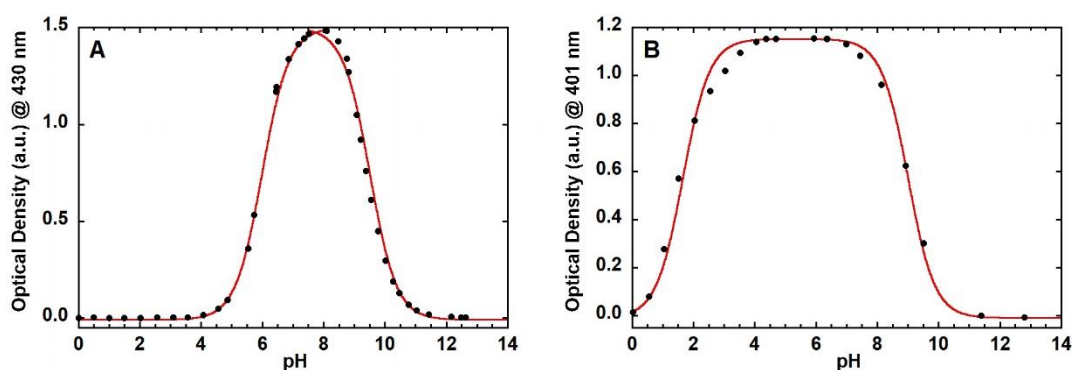


Figure 3. pH titration of complexes **1** (panel A) and **2** (panel B) measured on the LMCT (plain circles) together with fit (plain red lines). $[\text{LCu}(\text{solvent})]^{2+} = 0.2 \text{ mM}$, $[\text{SO}_3^{2-}] = [\text{S}_2\text{O}_3^{2-}] = 1 \text{ mM}$, AcN/HEPES (pH 6.5) 100 mM (50/50 v/v); $\ell = 1 \text{ cm}$. $T = 25^\circ\text{C}$.

Binding constants of SO_3^{2-} and $\text{S}_2\text{O}_3^{2-}$ to $[\text{LCu}(\text{solvent})]^{2+}$

The affinity of SO_3^{2-} and $\text{S}_2\text{O}_3^{2-}$ for **3** were determined by UV-Vis titration on the LMCT and d-d bands. Experiments at two concentrations were performed to (i) probe both transitions and (ii) to cover as much as possible the affinity range. They were performed in triplicate and both titrations on LMCT and d-d transitions were fitted (Figure 4). The apparent binding affinity values (^{app}Ka) obtained are given in Table 2. Two main observations can be made: at pH 6.5 the affinity of $\text{S}_2\text{O}_3^{2-}$ is about 10 times higher than that of SO_3^{2-} for $[\text{LCu}(\text{solvent})]^{2+}$ and is close to the one reported in case of $[(\text{L}_7)\text{Cu}(\text{H}_2\text{O})]^{2+}$ as the receiving complexes.²⁸

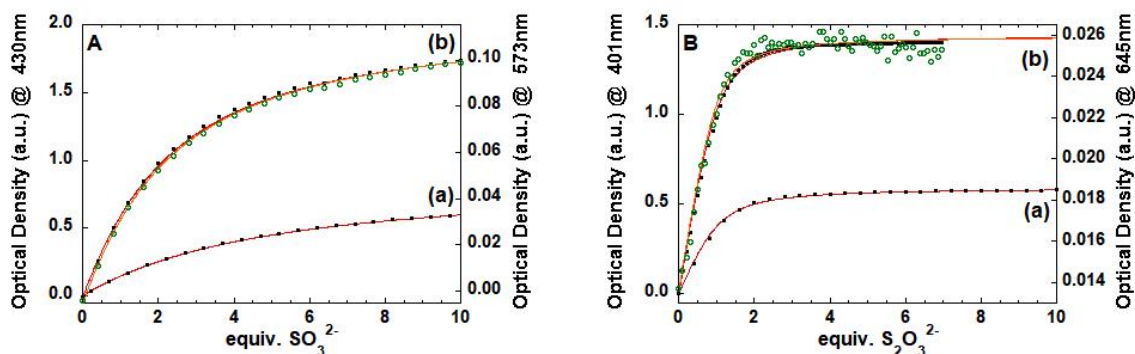


Figure 4. SO_3^{2-} (panel A) and $\text{S}_2\text{O}_3^{2-}$ (panel B) titrations into $[\text{LCu}(\text{solvent})]^{2+}$. Variations of the absorbance measured on the LMCT (black plain circles) or d-d bands (green open circles), at 0.1 mM (a) and 0.25 mM (b) concentration in $[\text{LCu}(\text{solvent})]^{2+}$, and corresponding fits (red lines: LMCT bands, orange line: d-d bands). AcN/HEPES (pH 6.5) 100mM (50/50 v/v); $l = 1\text{cm}$; $T = 25^\circ\text{C}$.

Cyclic voltammetry studies

The binding of SO_3^{2-} and $\text{S}_2\text{O}_3^{2-}$ was also probed by cyclic voltammetry (CV). Figure 5 shows the CV of complex **3** and upon addition of 1 to 5 equiv. of SO_3^{2-} and $\text{S}_2\text{O}_3^{2-}$. Complex **3** shows a reversible wave at $E_{1/2} = -0.21\text{ V}$ vs. SCE ($\Delta E^p = 120\text{ mV}$) corresponding to the Cu(II)/Cu(I) redox couple. This value lies in the range $[-0.4\text{ to }0\text{ V}]$ (vs. SCE) reported for $[\text{LCu}(\text{H}_2\text{O})]^{2+}$ and $[\text{LCu}(\text{AcN})]^{2+}$ in refs. ^{8, 21, 44} and ^{21, 45-47}, respectively, and mirrors the importance of solvation effects on redox potential values as well as the higher stabilization of $[\text{LCu}^{\text{I}}(\text{AcN})]^+$ in AcN and of $[\text{LCu}^{\text{II}}(\text{H}_2\text{O})]^{2+}$ in water medium. Upon addition of SO_3^{2-} and $\text{S}_2\text{O}_3^{2-}$ the redox potential is shifted towards more cathodic (negative) values in line with the substitution of a neutral solvent ligand by an anionic ligand in the Cu(II) complexes coordination sphere. The shift equals 40 mV for SO_3^{2-} and 60 mV for $\text{S}_2\text{O}_3^{2-}$ indicating a stronger stabilization by $\text{S}_2\text{O}_3^{2-}$ in agreement with the higher affinity determined previously and/or the higher negatively charged binding sulfur atom.

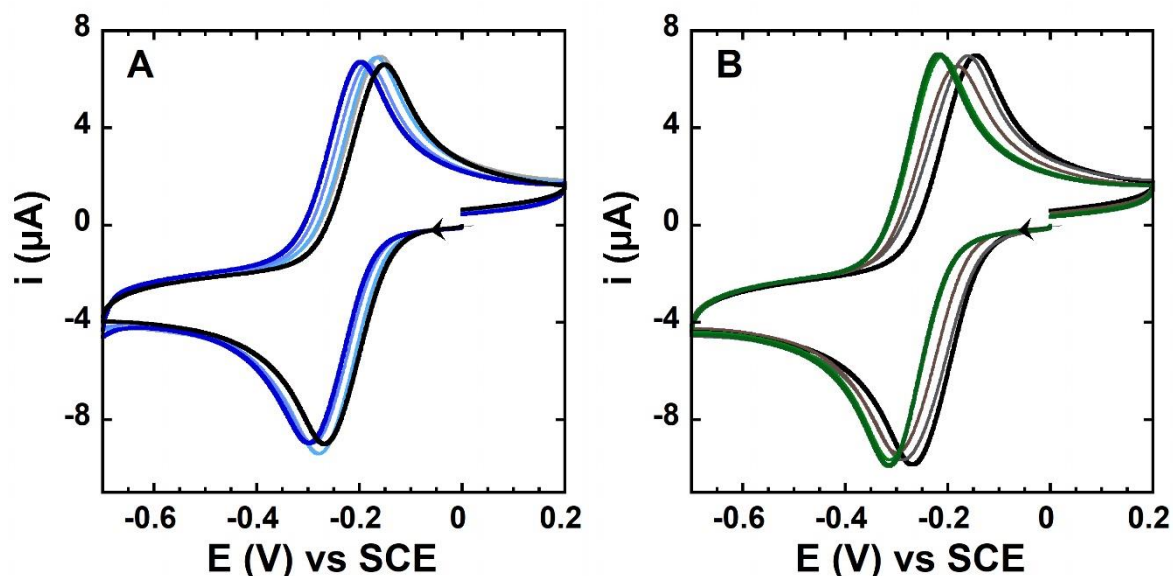


Figure 5. Cyclic voltammograms of $[\text{LCu}(\text{solvent})]^{2+}$ in presence of 0 (black line) to 5 equiv. of SO_3^{2-} (panel A, blue line) and $\text{S}_2\text{O}_3^{2-}$ (panel B, green line). AcN/HEPES (pH 6.5) 100mM (50/50 v/v), scan rate = $100 \text{ mV}\cdot\text{s}^{-1}$, working electrode = vitreous carbon, counter electrode: Pt, reference: SCE.

Determination of the sulfite concentration in sugar

As an application of the above described complexes characterizations, we determined the sulfite concentration in crystal sugar using the method of standard additions, by following the appearance of the LMCT band at 418 nm (see Table 1, Figure S1). The results are shown in Figure 6. The quantity of SO_3^{2-} in sugar was evaluated as 1.2 mg/kg of sugar (corresponding to a detection in the μM range). This indicates that this method although very simple and straightforward compares well with other methodologies developed for evaluation of SO_3^{2-} ,¹⁹ including colorimetric ones.⁴⁸⁻⁵⁴ SO_3^{2-} content in sugar was previously detected with other methods, which have, as the current method, a threshold level in the μM range as well.⁵⁵⁻⁵⁸

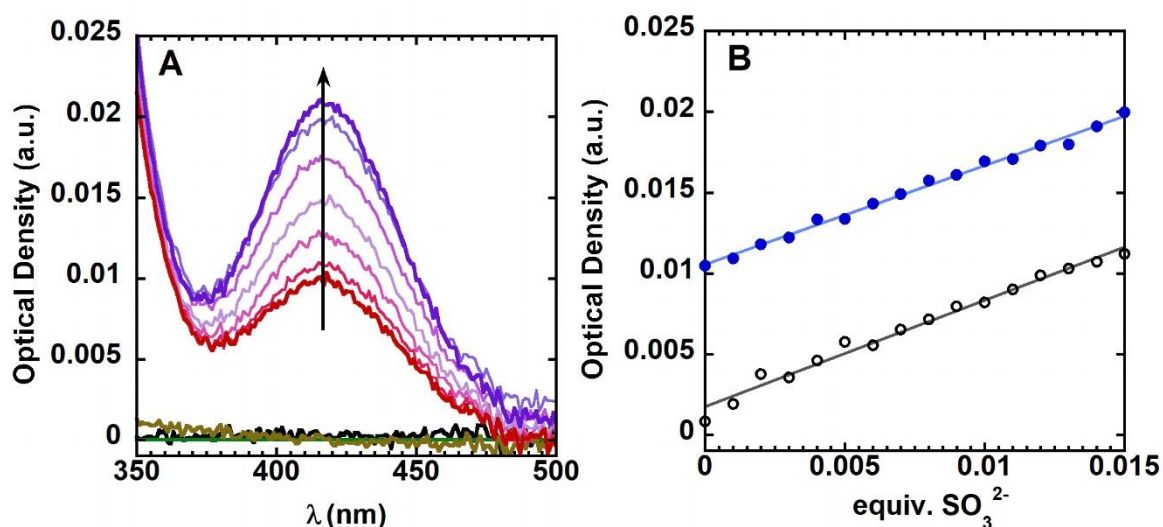


Figure 6. UV-Vis determination SO_3^{2-} level in sugar determined by the method of standard additions. (A) LMCT band of complex **1** in situ generated due to the presence of sugar (red bold line) and then as a function of controlled addition of SO_3^{2-} (up to 0.015 equiv. versus $[\text{LCu}(\text{H}_2\text{O})]^{2+}$, purple bold line). $[\text{LCu}(\text{H}_2\text{O})]^{2+} = 0.25 \text{ mM}$, $[\text{sugar}] = 0.4 \text{ g.mL}^{-1}$. (B) Titration curve and its linear fit ($y = 0.0105 + 0.61x$, $R = 0.997$, blue dots and line) together with the same titration curve without sugar (black open dots and grey line). Value of the intercept with the y-axis and slope releases the level of SO_3^{2-} in sugar.

Formation of **1** by reduction of **3** with dithionite

Sulfite binding to **3** was first observed upon addition of dithionite ($\text{S}_2\text{O}_4^{2-}$) to **3** whereas we aimed at forming in-situ the $[\text{LCu}^I(\text{solvent})]^+$ species in order to evaluate its reactivity towards dioxygen. The UV-Vis (especially the LMCT band) and EPR signatures that appeared were highly reminiscent of those of superoxide/hydroperoxide $[\text{LCu}(\text{II})]^{2+}$ adducts^{7, 11, 40-43} but were further attributed to formation of **1** by comparison with direct addition of SO_3^{2-} to **3**. **1** originates from the reduction of dithionite in the medium as described in scheme 1. The mechanism is based on the kinetic evolution of dithionite, and complexes **3** and **1** (Figure 7) and on refs.⁵⁹⁻⁶² about the various condition-dependent pathways of dithionite evolution. Briefly, dithionite ($\text{S}_2\text{O}_4^{2-}$) reacts with dioxygen to form sulfite (SO_3^{2-}), including in the stock solution of dithionite (reaction 1, scheme 1). In addition to this, likely minor way of producing sulfite ions, the reduction of **3** (or **1**) in the UV-Vis cuvette by dithionite leads to sulfite as a second product (reaction 2). In presence of **3** and sulfite, there is formation of **1**, which can be further reduced by dithionite (reaction 3) until dithionite is fully consumed. Hence, the first increase in the UV-Vis band at 418 nm (Table 1) corresponds to the formation of **1** along with reaction 1 (complex **3** to which is added dithionite from the stock solution, thus containing sulfite). Then and as long as there is still dithionite, **1** is formed but continuously reduced (no increase in the sulfite to Cu(II) LMCT band) in line with the respective redox potential of **1** (Table 1). Finally, once the concentration in dithionite is not enough to reduce **1**, **1** starts to accumulate. It is thus worth noting that dithionite in chemical or

biological experiments has to be carefully handled to avoid formation of undesired by-products including Cu(II) complexes.^{63, 64}

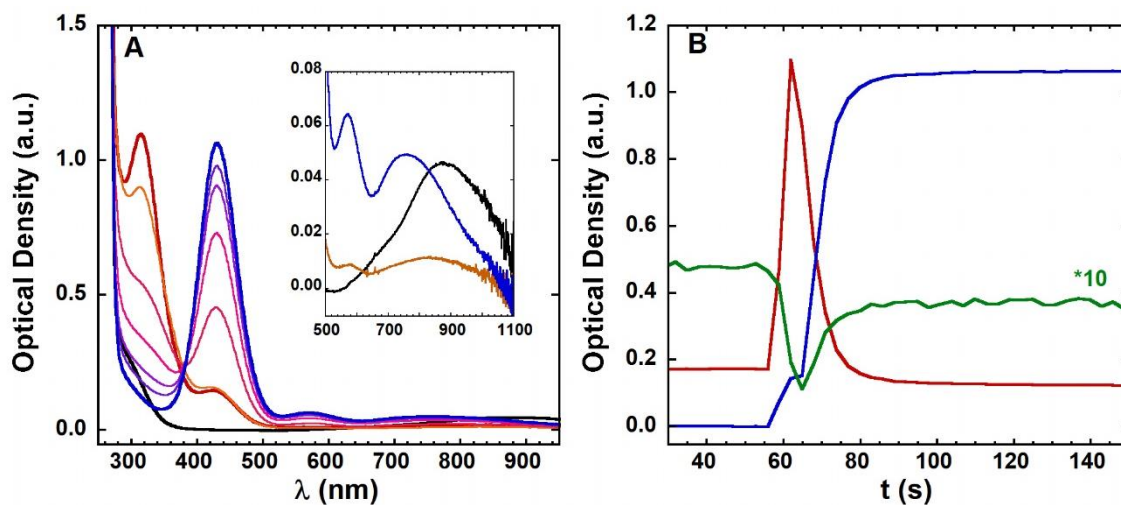
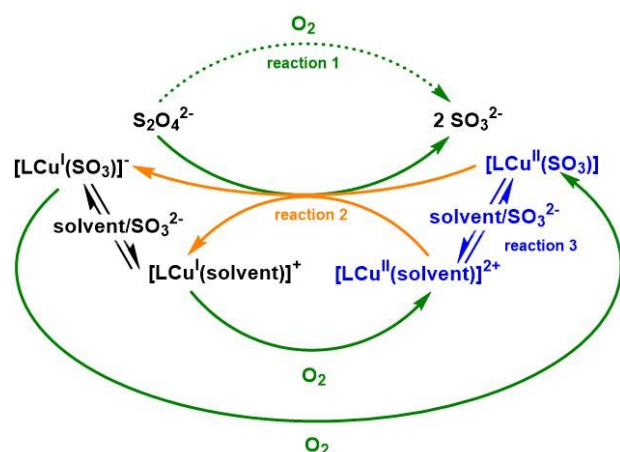


Figure 7. In situ formation of **1** by reduction of **3** with dithionite. Panel A: selection of key spectra (black: **3**, red: just after addition of dithionite and then orange to light blue: every 3s after addition of dithionite and blue: after completion of reaction), inset: d-d bands; panel B: kinetic monitoring at key wavelengths (315 nm in red, 430 nm in blue and 870 nm in green, intensity *10 to ease comparison with other kinetic traces). Dithionite was added at t = 56 s.

Scheme 1. Proposed mechanism for the formation of complex **1** from the aerobic reduction of **3** by dithionite.



Concluding remarks

In the present short report, we described the synthesis and full spectroscopic and analytic characterizations of two Cu(II) complexes obtained with the well-known TMPA (L) ligand, where the fifth coordination site is occupied either by a sulfite (SO_3^{2-}) or thiosulfate ($\text{S}_2\text{O}_3^{2-}$) ion. The in-situ formation of the $[\text{LCu}(\text{SO}_3)]$ complex was further used to evaluate the sulfite content in crystal sugar, in order to illustrate one possible application of the basic study shown here. It is here worth noting that in addition to be very easy to set up (commercial ligand, UV-Vis detection method, ratiometric), the threshold level of detection of the present method compares well with previous probes reported in the literature, including those relying on more indirect paths. Besides, because the UV-Vis depends on the nature of the adduct (here $[\text{LCu}(\text{SO}_3)]$ or $[\text{LCu}(\text{S}_2\text{O}_3)]$), the method is also specific for the detection of a given exogenous ligand.

The formation of $[\text{LCu}(\text{SO}_3)]$ was discovered by chance in the course of an experiment based on the aerobic reduction of $[(\text{L})\text{Cu}(\text{solvent})]^{2+}$ by dithionite, illustrating the complexity and hazard to use such reductant in Cu(II) chemistry. In the present case, however, it leads to the full analyses of the $[\text{LCu}(\text{SO}_3)]$ and parent $[\text{LCu}(\text{S}_2\text{O}_3)]$ complexes, including by X-ray crystallography.

Experimental Section

Chemicals.

CuSO₄•5(H₂O), sodium thiosulfate anhydrous, sodium dithionite, sodium hydroxide and HEPES buffer were purchased from Sigma (purity ≥ 98 %). Tris(2-pyridylmethyl)amine was purchased from TCI (purity ≥ 98 %). Sulfuric acid was bought from Fluka (purity 95.0-97.0 %). Sodium sulfite was purchased from Fluorochem. Every reagents was used without further purification. Acetonitrile (AcN) was purchased from Carlo Erba (HPLC isocratic grade).

Every aqueous solutions were prepared in ultrapure water with a resistivity of 18.2 MΩ·cm.

HEPES buffer: A 500 mM stock solution of HEPES buffer is prepared by dissolution of 5.98 g of HEPES in 50 mL H₂O. The pH is adjusted by addition of a stock solution of NaOH (5 M) drop by drop under stirring until pH 6.5 is reached.

Cu^{II}SO₄: A 100 mM stock solution of Cu^{II}SO₄ is prepared by dissolution of 1.25 g of Cu^{II}SO₄•5H₂O in 50 mL H₂O. Cu^{II} concentration was measured by UV-visible absorption (the absorbance was measured at 800 and 450 nm, the difference A₈₀₀–A₄₅₀ was used with ε=12 M⁻¹cm⁻¹ to determine the concentration). The solution was diluted down to 25 mM in Cu^{II} to form the final stock solution used further in experiments.

For EPR experiments, a ⁶⁵Cu(NO₃) stock solution was obtained from the nitric acid attack of a ⁶⁵Cu foil (Eurisotop).

TMPA ligand (L): A 10 mM stock solution of Tris(2-pyridylmethyl)amine (TMPA) is prepared by dissolution of 14.5 mg of TMPA in 50 mL H₂O. The exact concentration is determined by UV-vis titration using stock solution of Cu^{II}SO₄ and monitoring the absorbance at 890 nm corrected with the absorbance at 480 nm, see Figure S2).

Sodium sulfite (Na₂SO₃), sodium thiosulfate (Na₂S₂O₃) and sodium dithionite (Na₂S₂O₄) solutions are freshly prepared at the desired concentration by dissolution in H₂O just before use.

Crystallographic samples and data.

Formation of crystals of **1** and **2**. A 100 mM solution of **1** was prepared by mixing TMPA (1.1 eq; 32 mg) with Cu^{II}SO₄•5H₂O (1 eq; 25 mg) in 1 mL CH₃CN/HEPES (pH 6.5; 500 mM) 50/50 (v/v) (turquoise solution), then Na₂SO₃ (7 eq, 88 mg) was added (dark brown solution). The solution is sonicated and filtered. Dark green crystals suitable for X-ray crystallography were obtained by slow diffusion of diethylether into the filtrate at room temperature in the dark. A 100 mM solution of **2** was prepared, by mixing TMPA (1.1 eq; 32 mg) with Cu^{II}SO₄•5H₂O (1 eq; 25 mg) in 1 mL CH₃CN/HEPES (pH 6.5; 500

mM) 50/50 (v/v) (turquoise solution), then Na₂S₂O₃ (5 eq, 79 mg) was added (dark green solution). The solution is sonicated. Blue-greenish crystals suitable for characterization were obtained by slow diffusion of diethylether at room temperature in the dark.

Crystallographic data were collected at 273(2) K (**1**) or 110(2)K (**2**), on a Bruker-AXS Kappa APEX II diffractometer equipped with a 30W air-cooled microfocus source, using MoK_α radiation (λ=0.71073 Å). Phi- and omega-scans were used. Space groups were determined on the basis of systematic absences and intensity statistics. Empirical absorption correction was employed.¹The structures were solved using an intrinsic phasing method (SHELXT),² and refined using the least-squares method on *F*².³All non-H atoms were refined with anisotropic displacement parameters. The hydrogen atoms on carbon atoms were refined isotropically at calculated positions using the riding model. All hydrogen atoms of water molecules of **2** were located in the difference Fourier maps and refined freely.

CCDC-2068976 (**1**), CCDC-2068975 (**2**), contain the supplementary crystallographic data for this paper. These data can be obtained free of charge from The Cambridge Crystallographic Data Centre via www.ccdc.cam.ac.uk/data_request/cif.

UV-Visible spectroscopy.

The UV-vis were recorded on a Hewlett Packard Agilent 8453 or 8454 spectrophotometer at 25°C under a 800 rpm stirring.

-pH titration of **1** and **2**. The pH of a 0.2 mM solution **1** (resp. **2**) in situ generated by mixing [LCu(solvent)]²⁺ = 0.2 mM and [SO₃²⁻] = 1 mM or [S₂O₃²⁻] = 1 mM in AcN/HEPES (pH 6.5, 100 mM in aqueous phase) is varied by addition of H₂SO₄ or NaOH from stock solutions and monitored using a pH micro-electrode directly put in the UV-Vis cuvette. A UV-vis spectrum is recorded for each pH value and the absorbance at 430 nm (resp. 401 nm) monitored.

-Sulfite and thiosulfate titrations to **3**: To a 0.25 mM solution of **3** in AcN/HEPES (pH 6.5, 100 mM in aqueous phase) 50/50 (v/v), 1 μL of a freshly prepared 50 mM solution of Na₂SO₃ (0.1 eq, 25 μM) or Na₂SO₃ (0.1 eq, 25 μM) is added every 90 s by a automatic fluid dispenser and titration machine (Dostal Dosy) under stirring in an initial volume of 2 mL. A UV-Vis spectrum is recorded after each addition and further analyzed.

The titration curves were analyzed using a in-house procedure written in Kaleidagraph software.

Change in the absorbance at xyz nm (xyz stands for the maximum absorbance of the LMCT and d-d bands in **1** and **2**) was reproduced according to the following procedure.

Absorbance was calculated as a function SO₃²⁻ or S₂O₃²⁻ equivalent numbers according to:

$$Abs = [([3] - [\alpha]C_0) \cdot \epsilon_{xyz\ nm}^3 + [\alpha]C_0 \cdot \epsilon_{xyz\ nm}^1]l \text{ or } Abs = [([3] - [\alpha]C_0) \cdot \epsilon_{xyz\ nm}^3 + [\alpha]C_0 \cdot \epsilon_{xyz\ nm}^2]l$$

where α stands for the progression of the following reaction: $\underline{3} + \text{SO}_3^{2-} \rightarrow \underline{1}$ or $\underline{3} + \text{S}_2\text{O}_3^{2-} \rightarrow \underline{2}$

where the affinity constant was adjusted to obtain the best reproduction of the experimental data.

Fits of the LMCT and d-d bands were performed simultaneously to increase constraints of the affinity value.

Titration of sulfite in sugar: 1 g of crystal sugar was dissolved by addition of 1 mL of a 100 mM HEPES buffer solution at pH 6.5 affording a sugar stock solution of 2.5 mL. 25 mg of Na_2SO_3 was dissolved in 2 mL H_2O and diluted again just before use to afford a solution at 0.5 mM. A 3 mL UV-vis cuvette is loaded with 1924 μL of the crystal sugar stock solution. 60 μL of a 10 mM TMPA stock solution and 20 μL of a 25 mM Cu(II)SO_4 stock solution are added affording a total concentration of 0.25 mM $\text{Cu}^{\text{II}}\text{TMPA}$. 1 μL of a freshly prepared 0.5 mM solution of Na_2SO_3 (0.001 eq, 0.25 μM) is added every 60 s by a automatic fluid dispenser and titration machine (Dostal Dosy) under stirring. A UV-vis spectrum is recorded prior to each addition. The absorbance at 418 nm is monitored.

The absorption band at 418 nm of the $\underline{1}$ with sugar as source of SO_3^{2-} corresponds to 0.015 equivalent of Na_2SO_3 corresponding to a concentration of 3.75 μM in the UV-cuvette.

$$[\text{Na}_2\text{SO}_3]_{\text{stock solution}} = \frac{[\text{Na}_2\text{SO}_3]_{\text{UVcuvette}} * V_{\text{UVcuvette}}}{V_{\text{sucree}}}$$

$$[\text{Na}_2\text{SO}_3]_{\text{stock solution}} = \frac{3.75 * 10^{-6} * 2 * 10^{-3}}{1924 * 10^{-6}}$$

$$[\text{Na}_2\text{SO}_3]_{\text{stock solution}} = 3.90 \mu\text{M}$$

$$m_{\text{Na}_2\text{SO}_3\text{stock solution}} = [\text{Na}_2\text{SO}_3]_{\text{stock solution}} * V_{\text{stock solution}} * MW_{\text{Na}_2\text{SO}_3}$$

$$m_{\text{Na}_2\text{SO}_3\text{stock solution}} = 3.90 * 10^{-6} * 2.5 * 10^{-3} * 126.04$$

$$m_{\text{Na}_2\text{SO}_3\text{stock solution}} = 1.23 * 10^{-6} \text{ g per 1 g of sugar}$$

$$m_{\text{Na}_2\text{SO}_3\text{sugar}} = 1.23 \text{ mg/kg}$$

EPR spectroscopy.

Electron Paramagnetic Resonance (EPR) data were recorded using an Elexsys E 500 Bruker spectrometer, operating at a microwave frequency of approximately 9.5 GHz. Spectra were recorded using a microwave power of 5 mW across a sweep width of 200 mT (centered at 320 mT) with modulation amplitude of 0.5 mT. Experiments were carried out at 120 K using a liquid nitrogen cryostat.

Sample preparation for EPR experiments: the TMPA ligand was dissolved in water to have a final concentration at about 10 mM. The solution was diluted down to 0.55 mM in a mixture of AcN/HEPES (pH 6.5) 100 mM 50/50 (v/v) and 0.9 equivalent of $^{65}\text{Cu(II)NO}_3$ was added from stock solution. Depending to the EPR sample desired, 5 equivalents of Na_2SO_3 , or $\text{Na}_2\text{S}_2\text{O}_3$ were added. 200 μL of the solution was transferred to an EPR tube and frozen until used.

Cyclic voltammetry.

Cyclic voltammetry was performed in a standard three-electrode cell by using an Autolab potentiostat (PGSTAT302N, Autolab) interfaced to a PC computed and piloted with GPES software (version 4.9). A saturated calomel electrode, isolated from the solution by a glass frit, and a platinum wire were used as reference and counter electrodes, respectively. Working electrode was a glassy carbon electrode (3 mm diameter) polished by a 1 μm and 0.3 μm alumina slurry (2 min each) on a cloth polishing pad and washed with water under sonication (1 min). CVs were recorded under argon pressure passing through a bubbler containing AcN at room temperature. The cyclic voltammograms were recorded at a scan rate of 100 mV/s, with a step potential of 1 mV.

A 0.5 mM solution of **3** were in situ generated by mixing TMPA (1.5 eq; 0.75 mM) with $\text{Cu}^{\text{II}}\text{SO}_4 \cdot 5\text{H}_2\text{O}$ (1 eq; 0.5 mM,) in 6 mL $\text{CH}_3\text{CN}/\text{HEPES}$ (pH 6.5) 100 mM 50/50 (v/v), then 1 to 5 equivalents of Na_2SO_3 or $\text{Na}_2\text{S}_2\text{O}_3$ were added from 200 mM stock solution freshly prepared in H_2O .

Elemental analysis of 2.

A 100 mM solution of **2** was prepared in a mixture of AcN/HEPES 50/50 (v/v), by mixing TMPA (1.1 eq; 110 mM, 16 mg) with $\text{Cu}^{\text{II}}\text{SO}_4 \cdot 5\text{H}_2\text{O}$ (1 eq; 100 mM, 12.5 mg) (turquoise solution), then $\text{Na}_2\text{S}_2\text{O}_3$ (5 eq, 500 mM, 39.5 mg) is added (dark green solution). The solution is sonicated. A shiny dark blue-greenish powder is obtained by precipitation in diethylether and filtered. The powder is freeze-dried to afford 11.4 mg of **2** suitable for elemental analysis. Theoretical values for **2**, 0.12 $\text{Na}_2\text{S}_2\text{O}_3$: C (44.3); H (3.7) and N (11.5); experimental values: C (44.3); H (3.4) and N (11.5).

Acknowledgments.

L.B. thanks the University Paul Sabatier (UPS) for a PhD Fellowship allocated to the NAIST-UPS doctoral double degree program.

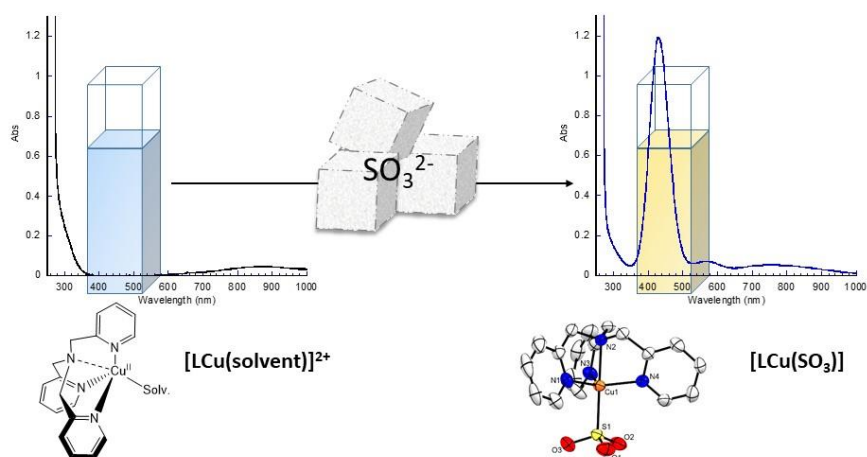
References.

1. Solomon, E. I.; Heppner, D. E.; Johnston, E. M.; Ginsbach, J. W.; Cirera, J.; Qayyum, M.; Kieber-Emmons, M. T.; Kjaergaard, C. H.; Hadt, R. G.; Tian, L., Copper Active Sites in Biology. *Chemical Reviews* **2014**, *114* (7), 3659-3853.
2. Wikström, M.; Sharma, V., Proton pumping by cytochrome c oxidase – A 40 year anniversary. *Biochimica et Biophysica Acta (BBA) - Bioenergetics* **2018**, *1859* (9), 692-698.
3. Reed, C. J.; Lam, Q. N.; Mirts, E. N.; Lu, Y., Molecular understanding of heteronuclear active sites in heme-copper oxidases, nitric oxide reductases, and sulfite reductases through biomimetic modelling. *Chemical Society Reviews* **2021**, *50* (4), 2486-2539.
4. Adam, S. M.; Wijeratne, G. B.; Rogler, P. J.; Diaz, D. E.; Quist, D. A.; Liu, J. J.; Karlin, K. D., Synthetic Fe/Cu Complexes: Toward Understanding Heme-Copper Oxidase Structure and Function. *Chemical Reviews* **2018**, *118* (22), 10840-11022.
5. Bravin, C.; Badetti, E.; Licini, G.; Zonta, C., Tris(2-pyridylmethyl)amines as emerging scaffold in supramolecular chemistry. *Coordination Chemistry Reviews* **2021**, *427*, 213558.
6. Smits, N. W. G.; van Dijk, B.; de Bruin, I.; Groeneveld, S. L. T.; Siegler, M. A.; Hetterscheid, D. G. H., Influence of Ligand Denticity and Flexibility on the Molecular Copper Mediated Oxygen Reduction Reaction. *Inorganic Chemistry* **2020**, *59* (22), 16398-16409.
7. Diaz, D. E.; Quist, D. A.; Herzog, A. E.; Schaefer, A. W.; Kipouros, I.; Bhadra, M.; Solomon, E. I.; Karlin, K. D., Impact of Intramolecular Hydrogen Bonding on the Reactivity of Cupric Superoxide Complexes with O-H and C-H Substrates. *Angewandte Chemie International Edition* **2019**, *58* (49), 17572-17576.
8. Langerman, M.; Hetterscheid, D. G. H., Fast Oxygen Reduction Catalyzed by a Copper(II) Tris(2-pyridylmethyl)amine Complex through a Stepwise Mechanism. *Angewandte Chemie International Edition* **2019**, *58* (37), 12974-12978.
9. Quist, D. A.; Ehudin, M. A.; Karlin, K. D., Unprecedented direct cupric-superoxo conversion to a bis- μ -oxo dicopper(III) complex and resulting oxidative activity. *Inorganica chimica acta* **2019**, *485*, 155-161.
10. Mehlich, F.; Roberts, A. E.; Kerscher, M.; Comba, P.; Lawrance, G. A.; Würtele, C.; Becker, J.; Schindler, S., Synthesis and characterization of copper complexes with a series of tripodal amine ligands. *Inorganica chimica acta* **2019**, *486*, 742-749.
11. Bhadra, M.; Lee, J. Y. C.; Cowley, R. E.; Kim, S.; Siegler, M. A.; Solomon, E. I.; Karlin, K. D., Intramolecular Hydrogen Bonding Enhances Stability and Reactivity of Mononuclear Cupric Superoxide Complexes. *Journal of the American Chemical Society* **2018**, *140* (29), 9042-9045.
12. Cheignon, C.; Jones, M.; Atrián-Blasco, E.; Kieffer, I.; Faller, P.; Collin, F.; Hureau, C., Identification of key structural features of the elusive Cu- $A\beta$ complex that generates ROS in Alzheimer's disease. *Chemical Science* **2017**, *8* (7), 5107-5118.
13. Atrián-Blasco, E.; Del Barrio, M.; Faller, P.; Hureau, C., Ascorbate Oxidation by Cu(Amyloid- β) Complexes: Determination of the Intrinsic Rate as a Function of Alterations in the Peptide Sequence Revealing Key Residues for Reactive Oxygen Species Production. *Analytical Chemistry* **2018**, *90* (9), 5909-5915.
14. Franco, R.; Navarro, G.; Martínez-Pinilla, E., Antioxidants versus Food Antioxidant Additives and Food Preservatives. *Antioxidants* **2019**, *8* (11), 542.
15. Kontaxakis, E.; Trantas, E.; Ververidis, F., Resveratrol: A Fair Race Towards Replacing Sulfites in Wines. *Molecules* **2020**, *25* (10), 2378.

16. McGeer, P. L.; McGeer, E. G.; Lee, M., Medical uses of Sodium thiosulfate. *Journal of Neurology & Neuromedicine* **2016**, *1* (3), 28-30.
17. Skypala, I. J.; Williams, M.; Reeves, L.; Meyer, R.; Venter, C., Sensitivity to food additives, vaso-active amines and salicylates: a review of the evidence. *Clinical and Translational Allergy* **2015**, *5* (1), 34.
18. Summary of evaluations performed by the Joint FAO/WHO Expert Committee on Food Additives. Sulfur dioxide. . Rome, Italy and Geneva, Switzerland.: Food and Agriculture Organization/World Health Organization, 2007.
19. Pundir, C. S.; Rawal, R., Determination of sulfite with emphasis on biosensing methods: a review. *Analytical and Bioanalytical Chemistry* **2013**, *405* (10), 3049-3062.
20. Porras Gutiérrez, A. G.; Zeitouny, J.; Gomila, A.; Douziech, B.; Cosquer, N.; Conan, F.; Reinaud, O.; Hapiot, P.; Le Mest, Y.; Lagrost, C.; Le Poul, N., Insights into water coordination associated with the Cull/Cul electron transfer at a biomimetic Cu centre. *Dalton Transactions* **2014**, *43* (17), 6436-6445.
21. Nagao, H.; Komeda, N.; Mukaida, M.; Suzuki, M.; Tanaka, K., Structural and Electrochemical Comparison of Copper(II) Complexes with Tripodal Ligands. *Inorganic Chemistry* **1996**, *35* (23), 6809-6815.
22. Guo, H.; Gong, C.; Zeng, X.; Xu, H.; Zeng, Q.; Zhang, J.; Zhong, Z.; Xie, J., Isopolymolybdate-based inorganic–organic hybrid compounds constructed by multidentate N-donor ligands: syntheses, structures and properties. *Dalton Transactions* **2019**, *48* (17), 5541-5550.
23. Bazley, I. J.; Erie, E. A.; Feiereisel, G. M.; LeWarne, C. J.; Peterson, J. M.; Sandquist, K. L.; Oshin, K. D.; Zeller, M., X-ray Crystallography Analysis of Complexes Synthesized with Tris(2-pyridylmethyl)amine: A Laboratory Experiment for Undergraduate Students Integrating Interdisciplinary Concepts and Techniques. *Journal of Chemical Education* **2018**, *95* (5), 876-881.
24. Massoud, S. S.; Louka, F. R.; Gazzaz, M. A.; Henary, M. M.; Fischer, R. C.; Mautner, F. A., Polynuclear copper(II) complexes bridged by polycarboxylates of aromatic and N-heterocyclic compounds. *Polyhedron* **2016**, *111*, 45-52.
25. Lim, B. S.; Holm, R. H., Molecular Heme–Cyanide–Copper Bridged Assemblies: Linkage Isomerism, Trends in ν_{CN} Values, and Relation to the Heme- $\alpha 3$ /CuB Site in Cyanide-Inhibited Heme–Copper Oxidases. *Inorganic Chemistry* **1998**, *37* (19), 4898-4908.
26. Ward, A. L.; Elbaz, L.; Kerr, J. B.; Arnold, J., Nonprecious Metal Catalysts for Fuel Cell Applications: Electrochemical Dioxygen Activation by a Series of First Row Transition Metal Tris(2-pyridylmethyl)amine Complexes. *Inorganic Chemistry* **2012**, *51* (8), 4694-4706.
27. Fujii, T.; Naito, A.; Yamaguchi, S.; Wada, A.; Funahashi, Y.; Jitsukawa, K.; Nagatomo, S.; Kitagawa, T.; Masuda, H., Construction of a square-planar hydroperoxo-copper(ii) complex inducing a higher catalytic reactivity. *Chemical Communications* **2003**, (21), 2700-2701.
28. Fischmann, A. J.; Warden, A. C.; Black, J.; Spiccia, L., Synthesis, Characterization, and Structures of Copper(II)–Thiosulfate Complexes Incorporating Tripodal Tetraamine Ligands. *Inorganic Chemistry* **2004**, *43* (21), 6568-6578.
29. Addison, A. W.; Rao, T. N.; Reedijk, J.; van Rijn, J.; Verschoor, G. C., Synthesis, structure, and spectroscopic properties of copper(II) compounds containing nitrogen–sulphur donor ligands; the crystal and molecular structure of aqua[1,7-bis(N-methylbenzimidazol-2'-yl)-2,6-dithiaheptane]copper(II) perchlorate. *Journal of the Chemical Society, Dalton Transactions* **1984**, (7), 1349-1356.
30. Fischmann, A. J.; Forsyth, C. M.; Spiccia, L., Stabilization of Copper(II) Thiosulfonate Coordination Complexes Through Cooperative Hydrogen Bonding Interactions. *Inorganic Chemistry* **2008**, *47* (22), 10565-10574.
31. Garribba, E.; Micera, G., The Determination of the Geometry of Cu(II) Complexes: An EPR Spectroscopy Experiment. *Journal of Chemical Education* **2006**, *83* (8), 1229.
32. Kokoszka, G.; Karlin, K. D.; Padula, F.; Baranowski, J.; Goldstein, C., EPR of copper(II) complexes with tripodal ligands: dynamical properties. *Inorganic Chemistry* **1984**, *23* (25), 4378-4380.

33. Q., E. M.; Yasunori, O.; Seigo, Y.; Masamoto, I., EPR and ENDOR Study of Trigonal Bipyramidal Copper Complexes with a Nitrogen Donor Tripodal Ligand. *Bulletin of the Chemical Society of Japan* **1996**, *69* (8), 2201-2209.
34. Duggan, M.; Ray, N.; Hathaway, B.; Tomlinson, G.; Brint, P.; Pelin, K., Crystal structure and electronic properties of ammine[tris(2-aminoethyl)amine]copper(II) diperchlorate and potassium penta-amminecopper(II) tris(hexafluorophosphate). *Journal of the Chemical Society, Dalton Transactions* **1980**, (8), 1342-1348.
35. Paria, S.; Morimoto, Y.; Ohta, T.; Okabe, S.; Sugimoto, H.; Ogura, T.; Itoh, S., Copper(I)–Dioxygen Reactivity in the Isolated Cavity of a Nanoscale Molecular Architecture. *European Journal of Inorganic Chemistry* **2018**, *2018* (19), 1976-1983.
36. Suspène, C.; Brandès, S.; Guillard, R., Reversible Coordination of Dioxygen by Tripodal Tetraamine Copper Complexes Incorporated in a Porous Silica Framework. *Chemistry – A European Journal* **2010**, *16* (21), 6352-6364.
37. Izzet, G.; Zeng, X.; Akdas, H.; Marrot, J.; Reinaud, O., Drastic effects of the second coordination sphere on neutral vs. anionic guest binding to a biomimetic Cu(ii) center embedded in a calix[6]aza-cryptand. *Chemical Communications* **2007**, (8), 810-812.
38. Le Poul, N.; Douziech, B.; Zeitouny, J.; Thiabaud, G.; Colas, H.; Conan, F.; Cosquer, N.; Jabin, I.; Lagrost, C.; Hapiot, P.; Reinaud, O.; Le Mest, Y., Mimicking the Protein Access Channel to a Metal Center: Effect of a Funnel Complex on Dissociative versus Associative Copper Redox Chemistry. *Journal of the American Chemical Society* **2009**, *131* (49), 17800-17807.
39. Thiabaud, G.; Brugnara, A.; Carboni, M.; Le Poul, N.; Colasson, B.; Le Mest, Y.; Reinaud, O., Synthesis and Studies of a Water-Soluble and Air-Stable CuI/CuII Open-Shell Funnel Complex. *Organic Letters* **2012**, *14* (10), 2500-2503.
40. Kim, S.; Saracini, C.; Siegler, M. A.; Drichko, N.; Karlin, K. D., Coordination Chemistry and Reactivity of a Cupric Hydroperoxide Species Featuring a Proximal H-Bonding Substituent. *Inorganic Chemistry* **2012**, *51* (23), 12603-12605.
41. Choi, Y. J.; Cho, K.-B.; Kubo, M.; Ogura, T.; Karlin, K. D.; Cho, J.; Nam, W., Spectroscopic and computational characterization of CuII–OOR (R = H or cumyl) complexes bearing a Me6-tren ligand. *Dalton Transactions* **2011**, *40* (10), 2234-2241.
42. Maiti, D.; Lee, D.-H.; Gaoutchenova, K.; Würtele, C.; Holthausen, M. C.; Narducci Sarjeant, A. A.; Sundermeyer, J.; Schindler, S.; Karlin, K. D., Reactions of a Copper(II) Superoxo Complex Lead to C–H and O–H Substrate Oxygenation: Modeling Copper-Monooxygenase C–H Hydroxylation. *Angewandte Chemie International Edition* **2008**, *47* (1), 82-85.
43. Fujii, T.; Yamaguchi, S.; Funahashi, Y.; Ozawa, T.; Tosha, T.; Kitagawa, T.; Masuda, H., Mononuclear copper(ii)–hydroperoxo complex derived from reaction of copper(i) complex with dioxygen as a model of D β M and PHM. *Chemical Communications* **2006**, (42), 4428-4430.
44. Asahi, M.; Yamazaki, S.-i.; Itoh, S.; Ioroi, T., Electrochemical reduction of dioxygen by copper complexes with pyridylalkylamine ligands dissolved in aqueous buffer solution: the relationship between activity and redox potential. *Dalton Transactions* **2014**, *43* (28), 10705-10709.
45. Eckenhoff, W. T.; Garrity, S. T.; Pintauer, T., Highly Efficient Copper-Mediated Atom-Transfer Radical Addition (ATRA) in the Presence of Reducing Agent. *European Journal of Inorganic Chemistry* **2008**, *2008* (4), 563-571.
46. Zhang, C. X.; Kaderli, S.; Costas, M.; Kim, E.-i.; Neuhold, Y.-M.; Karlin, K. D.; Zuberbühler, A. D., Copper(I)–Dioxygen Reactivity of [(L)CuI]+ (L = Tris(2-pyridylmethyl)amine): Kinetic/Thermodynamic and Spectroscopic Studies Concerning the Formation of Cu–O₂ and Cu₂–O₂ Adducts as a Function of Solvent Medium and 4-Pyridyl Ligand Substituent Variations. *Inorganic Chemistry* **2003**, *42* (6), 1807-1824.
47. Chuang, C.-L.; dos Santos, O.; Xu, X.; Canary, J. W., Synthesis and Cyclic Voltammetry Studies of Copper Complexes of Bromo- and Alkoxyphenyl-Substituted Derivatives of Tris(2-pyridylmethyl)amine: Influence of Cation–Alkoxy Interactions on Copper Redox Potentials. *Inorganic Chemistry* **1997**, *36* (9), 1967-1972.

48. Ma, Y.; Fu, X.; He, W.; Gao, X., A label free colorimetric assay for detection of sulfite root based on Cu²⁺. *IOP Conference Series: Materials Science and Engineering* **2020**, *729*, 012090.
49. Chi, M.; Zhu, Y.; Jing, L.; Wang, C.; Lu, X., Fabrication of oxidase-like polyaniline-MnO₂ hybrid nanowires and their sensitive colorimetric detection of sulfite and ascorbic acid. *Talanta* **2019**, *191*, 171-179.
50. Xiang, K.; Chang, S.; Feng, J.; Li, C.; Ming, W.; Liu, Z.; Liu, Y.; Tian, B.; Zhang, J., A colorimetric and ratiometric fluorescence probe for rapid detection of SO₂ derivatives bisulfite and sulfite. *Dyes and Pigments* **2016**, *134*, 190-197.
51. Qin, W.; Su, L.; Yang, C.; Ma, Y.; Zhang, H.; Chen, X., Colorimetric Detection of Sulfite in Foods by a TMB–O₂–Co₃O₄ Nanoparticles Detection System. *Journal of Agricultural and Food Chemistry* **2014**, *62* (25), 5827-5834.
52. Zhang, J.; Xu, X.; Yang, X., Role of Tris on the colorimetric recognition of anions with melamine-modified gold nanoparticle probe and the visual detection of sulfite and hypochlorite. *Analyst* **2012**, *137* (15), 3437-3440.
53. Xu, J.; Liu, K.; Di, D.; Shao, S.; Guo, Y., A selective colorimetric chemosensor for detecting SO₃²⁻ in neutral aqueous solution. *Inorganic Chemistry Communications* **2007**, *10* (6), 681-684.
54. Venkatachalam, K.; Asaithambi, G.; Rajasekaran, D.; Periasamy, V., A novel ratiometric fluorescent probe for “naked-eye” detection of sulfite ion: Applications in detection of biological SO₃²⁻ ions in food and live cells. *Spectrochimica Acta Part A: Molecular and Biomolecular Spectroscopy* **2020**, *228*, 117788.
55. Jiang, X.; Xu, J.; Zhang, Y.; Wang, H.; Zeng, L.; Zhang, Y., A colorimetric and ratiometric fluorescent probe for the rapid and sensitive detection of sulfite in sugar. *Analytical Methods* **2016**, *8* (7), 1572-1576.
56. Feng, H.; Liu, J.; Qaitoon, A.; Meng, Q.; Sultanbawa, Y.; Zhang, Z.; Xu, Z. P.; Zhang, R., Responsive small-molecule luminescence probes for sulfite/bisulfite detection in food samples. *TrAC Trends in Analytical Chemistry* **2021**, *136*, 116199.
57. Zeng, R.-F.; Lan, J.-S.; Wu, T.; Liu, L.; Liu, Y.; Ho, R. J. Y.; Ding, Y.; Zhang, T., A novel mitochondria-targeted near-infrared fluorescent probe for selective and colorimetric detection of sulfite and its application in vitro and vivo. *Food Chemistry* **2020**, *318*, 126358.
58. Zhang, G.; Ji, R.; Kong, X.; Ning, F.; Liu, A.; Cui, J.; Ge, Y., A FRET based ratiometric fluorescent probe for detection of sulfite in food. *RSC Advances* **2019**, *9* (2), 1147-1150.
59. Read, J. F.; John, J.; MacPherson, J.; Schaubel, C.; Theriault, A., The kinetics and mechanism of the oxidation of inorganic oxysulfur compounds by potassium ferrate.: Part I. Sulfite, thiosulfate and dithionite ions. *Inorganica chimica acta* **2001**, *315* (1), 96-106.
60. Singh, D. K.; Sharma, R. N.; Srivastava, R. D., Kinetics of oxidation of sodium dithionite by flow thermal method. *AIChE Journal* **1978**, *24* (2), 232-237.
61. Wayman, M.; Lem, W. J., Decomposition of aqueous dithionite. Part II. A reaction mechanism for the decomposition of aqueous sodium dithionite. *Canadian Journal of Chemistry* **1970**, *48* (5), 782-787.
62. Burlamacchi, L.; Guarini, G.; Tiezzi, E., Mechanism of decomposition of sodium dithionite in aqueous solution. *Transactions of the Faraday Society* **1969**, *65* (0), 496-502.
63. Abreu, C. M. R.; Fu, L.; Carmali, S.; Serra, A. C.; Matyjaszewski, K.; Coelho, J. F. J., Aqueous SARA ATRP using Inorganic Sulfites. *Polym Chem* **2017**, *8* (2), 375-387.
64. Blackburn, N. J.; Strange, R. W.; Carr, R. T.; Benkovic, S. J., X-ray absorption studies of the copper-dependent phenylalanine hydroxylase from *Chromobacterium violaceum*. Comparison of the copper coordination in oxidized and dithionite-reduced enzymes. *Biochemistry* **1992**, *31* (23), 5298-5303.



The well-known $[(\text{TMPA})\text{Cu}]^{2+}$ moiety was used to detect sulfite ions (SO_3^{2-}) from crystal sugar while the X-ray structure of a $[(\text{ligand})\text{Cu}(\text{SO}_3)]$ complex was determined for the first time. Comparison of $[(\text{TMPA})\text{Cu}(\text{SO}_3)]$ properties with those of the parent $[(\text{TMPA})\text{Cu}(\text{S}_2\text{O}_3)]$ species is also reported.

Highlights.

- First crystal structure of copper(II) complex bounded to sulfite
- Selective, ratiometric and colorimetric detection of thiosulfate and sulfite
- Characterizations and speciation of copper(II)-sulfite and copper(II)-thiosulfate complexes
- Sulfite detection and quantification in crystal sugar sample
- Dithionite degradation products, such as sulfite can bind to copper(II) complexes